Neurobiology of Disease

Zn^{2+} Influx Is Critical for Some Forms of Spreading Depression in Brain Slices

Robert M. Dietz,[1] John H. Weiss,[2,3] and Claude W. Shuttleworth[1]

[1]Department of Neurosciences, University of New Mexico School of Medicine, Albuquerque, New Mexico 87131, and Departments of [2]Neurology and [3]Anatomy and Neurobiology, University of California, Irvine, Irvine, California 92697

Spreading depression (SD) is wave of profound depolarization that propagates throughout brain tissue and can contribute to the spread of injury after stroke or traumatic insults. The contribution of Ca^{2+} influx to SD differs depending on the stimulus, and we show here that Zn^{2+} can play a critical complementary role in murine hippocampal slices. In initial studies, we used the Na^+/K^+ ATPase inhibitor ouabain and found conditions in which SD was always prevented by L-type Ca^{2+} channel blockers; however, Ca^{2+} influx was not responsible for L-type effects. Cytosolic Ca^{2+} increases were not detectable in CA1 neurons before SD, and removal of extracellular Ca^{2+} did not prevent ouabain-SD. In contrast, cytosolic Zn^{2+} increases were observed in CA1 neurons before ouabain-SD, and L-type channel block prevented the intracellular Zn^{2+} rises. A slow mitochondrial depolarization observed before ouabain-SD was abolished by L-type channel block, and Zn^{2+} accumulation contributed substantially to initial mitochondrial depolarizations. Selective chelation of Zn^{2+} with *N*,*N*,*N*′,*N*′-tetrakis(2-pyridylmethyl)ethylenediamine (TPEN) abolished SD, implying that Zn^{2+} entry can play a critical role in the generation of ouabain-SD. TPEN was most effective when synaptic activity was reduced by adenosine A_1 receptor activation, and a combination of Ca^{2+} and Zn^{2+} removal was required to prevent ouabain-SD when A_1 receptors were blocked. Similarly, Zn^{2+} chelation could prevent SD triggered by oxygen/glucose deprivation but Zn^{2+} accumulation did not contribute to SD triggered by localized high K^+ exposures. These results identify Zn^{2+} as a new target for the block of spreading depolarizations after brain injury.

Key words: **hippocampal slice; mitochondria; spreading depression; calcium channels; zinc; ouabain**

Introduction

Spreading depression (SD) is characterized as a wave of severe depolarization that spreads throughout CNS tissues at a rate of several millimeters per second. SD can be triggered by brief exposures to elevated extracellular K^+, strong synaptic stimulation, inhibitors of Na^+/K^+ ATPase activity (e.g., ouabain), or ischemia models (Somjen, 2001). SD-like events are thought to be involved in the spread of injury after ischemic and traumatic brain injuries, and also contribute to migraine aura (Hossmann, 1996; Hadjikhani et al., 2001; Somjen, 2001; Hartings et al., 2003; Church and Andrew, 2005; Umegaki et al., 2005).

Large persistent intracellular Ca^{2+} increases follow SD, and it is clear that these increases contribute to neuronal death after some stimuli (Somjen, 2001). The contribution of Ca^{2+} to the initiation of SD is more complex, because Ca^{2+} accumulation is not required for initiation or progression of the SD event itself, at least when it is triggered in *in vitro* ischemia models or by ouabain (Ramos, 1975; Rader and Lanthorn, 1989; Young and Somjen, 1992; Basarsky et al., 1998; Somjen, 2001). However, SD generated by localized high K^+ stimuli does appear to involve Ca^{2+} (Footitt and Newberry, 1998; Peters et al., 2003), likely because of influx via presynaptic P/Q type channels and stimulation of transmitter release (Ayata et al., 2000). Here, we examined whether Zn^{2+} accumulation might contribute to the initiation of SD, especially in cases in which Ca^{2+} removal is without effect.

Zn^{2+} can enter cells through several routes, including Ca^{2+} channels, and induce neuronal injury (Koh et al., 1996; Choi and Koh, 1998; Weiss et al., 2000; Calderone et al., 2004). Zn^{2+} can accumulate in mitochondria (Sensi et al., 1999; Jiang et al., 2001; Malaiyandi et al., 2005), and mitochondrial dysfunction has in turn been suggested to contribute to induction of some forms of SD (Bahar et al., 2000; Hashimoto et al., 2000; Gerich et al., 2006). A large and rapid mitochondrial depolarization has been reported coincident with SD generated by hypoxia, but a slow progressive mitochondrial depolarization was also noted before the onset of SD (Bahar et al., 2000). Because these effects were not prevented by the removal of extracellular Ca^{2+} (Bahar et al., 2000), we also examined the possibility that mitochondrial depolarization before SD could instead be a consequence of Zn^{2+} increases.

We examined first SD induced by the Na^+/K^+ ATPase inhibitor ouabain and report conditions in which L-type Ca^{2+} channel activation is essential for SD, and also for the mitochondrial depolarization that precedes ouabain-SD. Additional observations provide evidence that influx of Zn^{2+} rather than Ca^{2+} can be critically responsible for the onset of ouabain-SD. The relevance

Received Oct. 11, 2007; revised June 12, 2008; accepted June 17, 2008.

This work was supported by National Institutes of Health Grants NS051288 (C.W.S.) and NS36548 (J.H.W.). We thank Drs. J. A. Connor and C. F. Valenzuela for helpful comments on the experiments and this manuscript.

Correspondence should be addressed to Dr. Claude W. Shuttleworth, Department of Neurosciences, MSC08 4740, University of New Mexico School of Medicine, 1 University of New Mexico, Albuquerque, NM 87131-0001. E-mail: bshuttleworth@salud.unm.edu.

DOI:10.1523/JNEUROSCI.0765-08.2008

 0270-6474/08/288014-11$15.00/0

of this finding to other forms of SD was also tested and we show that Zn^{2+} accumulation is not required for SD generated by localized high K^+ applications, but is an important contributor to SD in an *in vitro* model of ischemic injury. Some results have been presented in abstract form (Dietz et al., 2007a).

Materials and Methods

Slice preparation. Male FVB/N mice were obtained from Harlan and were housed in standard conditions (12/12 h light/dark cycle) before being killed at 4–6 weeks of age. All procedures were performed in accordance with the National Institutes of Health guidelines for the humane treatment of laboratory animals, and the protocol for these procedures was reviewed annually by the Institutional Animal Care and Use Committee at the University of New Mexico School of Medicine. Acute slices (350 μm) were prepared as previously described (Dietz et al., 2007b). After cutting and holding for 1 h at 35°C, artificial CSF (ACSF) was changed, and slices were held at room temperature until used for recording. Individual slices were transferred to the recording chamber and were superfused with oxygenated ACSF at 2 ml/min. The recording temperature was maintained within 0.5°C by using a feedback controller (Warner TC344B) and was 30–35°C, depending on the specific experiments (see Results). Spontaneous burst-like or SD-like depolarizations were not observed under these recording conditions, and (except where noted for localized high-K^+ applications) only a single challenge to a SD-triggering agent was tested in each slice.

Recording. Extracellular measurements of DC potentials were made using borosilicate glass microelectrodes, filled with ACSF (~5 MΩ) and placed in stratum radiatum ~50 μm below the surface of the slice. Ca^{2+} and Zn^{2+} measurements were made from individual CA1 pyramidal neurons. The procedures for intracellular recording/indicator injection were as described previously (Dietz et al., 2007b), with some modifications. Impalements were made using the step function of a Sutter manipulator (MP-225; Sutter Instrument), and neurons were visualized using a water-immersion objective [40×; numerical aperture (NA), 0.8; Olympus]. Neurons were impaled with sharp glass microelectrodes (initial resistance, ~100–120 MΩ) containing charged fluorescent indicators for either Ca^{2+} (fura-2 or fura-6F) or Zn^{2+} (FluoZin-3). Microelectrodes were tip-filled with 10 mM indicator in 0.5 M KAc/0.5 M KCl, back-filled with 3 M KCl, and indicator was injected by passing hyperpolarizing current (350–450 pA; 10 min). In experiments coloading fura-6F and FluoZin-3, electrodes tips contained 5 mM of each indicator. All neurons included in the study showed stable resting potentials more negative than −60 mV and responded to depolarizing current pulses with trains of overshooting action potentials and Ca^{2+} transients, as described previously with these recording conditions (Shuttleworth and Connor, 2001; Dietz et al., 2007b). In all experiments, the recording/filling electrode was then slowly withdrawn (in 1–2 μm steps, applied every 10–15 s) from the neuron. Electrode withdrawal was monitored from the amplitude of evoked action potentials evoked by applying depolarizing test pulses (100 ms, 200 pA; every 10 s). When action potential amplitude had reduced to less than ~20% of initial amplitude, a small membrane bleb had formed and withdrawal was paused. The impalement was then either spontaneously lost, or the electrode withdrawn with additional steps. Cytosolic Ca^{2+} levels were monitored throughout, and any neuron showing demonstrable Ca^{2+} increases during this procedure were discarded from the study. After electrode withdrawal, cells were allowed to recover for 20 min before application of any stimulus. Because high-resistance intracellular recording/filling electrodes were used, this procedure did not result in indicator leak or extracellular accumulation of any of the indicators examined.

Fura-2 and fura-6F were excited at 350/380 nm (400 nm dichroic; 50 ms) and emission detected at 510/50 nm using a monochromator-based imaging system (TILL Photonics, with Imago VGA CCD camera). FluoZin-3 was excited at 495 nm (505 nm dichroic; 15 ms), and emission was detected at 535/50 nm. When near-simultaneous fura-6F/FluoZin-3 measurements were made, coloaded neurons were excited sequentially at 350/380/495 nm (505 nm dichroic; 120/120/20 ms exposures) and emission of both indicators was detected at 535/50 nm. Estimation of Ca^{2+} concentrations and preparation of figures was as previously described (Shuttleworth and Connor, 2001; Dietz et al., 2007b).

Changes in mitochondrial potential were assessed using slices bulk-loaded with rhodamine 123 (Rh123). Slices were exposed to 26 μM Rh123 for 30 min at room temperature in a holding chamber before transfer to recording platform where the slices were washed with ACSF for 30 min before experimentation. Under these conditions, Rh123 is in the "quenched" mode, in which fluorescence increases are interpreted as mitochondrial depolarizations. Because of its relatively slow kinetics, mitochondrial Rh123 signals are not significantly complicated by plasma membrane effects under these conditions (Duchen et al., 2003). Fluorescence was excited at 488 nm, and emission was detected at 535/50 nm. The progression of SD was also monitored in some experiments by using autofluorescence excited at 360 nm (emission, >420 nm), as described previously (Shuttleworth and Connor, 2001). A 10× water-immersion objective (NA 0.3; Olympus) was used for Rh123 and autofluorescence imaging studies, which provided a field of view of ~840 μm centered in area CA1. This region was not sufficient to assess progression of events into adjacent hippocampal subregions, such as area CA3.

Reagents and solutions. Slice cutting solution contained the following (in mM): 2 KCl, 1.25 NaH_2PO_4, 6 $MgSO_4$, 26 $NaHCO_3$, 0.2 $CaCl_2$, 10 glucose, 220 sucrose, and 0.43 ketamine. ACSF contained the following (in mM): 126 NaCl, 2 KCl, 1.25 NaH_2PO_4, 1 $MgSO_4$, 26 $NaHCO_3$, 2 $CaCl_2$, and 10 glucose, and was equilibrated with 95%O_2/5%CO_2. Cutting and recording solutions were both 315–320 mOsm. ACSF was modified in zero-Ca^{2+} experiments by replacement of $CaCl_2$ with $MgSO_4$, and addition of chelators (0.5 mM EGTA or 1 mM BAPTA, as described below). In oxygen/glucose deprivation (OGD) experiments, ACSF was modified by equimolar replacement of glucose with sucrose, and equilibrated with 95% N_2/5% CO_2.

Fluorescent indicators and *N*,*N*,*N*′,*N*′-tetrakis(2-pyridylmethyl)-ethylenediamine (TPEN) were obtained from Invitrogen, and all other reagents were obtained from Sigma-Aldrich. Ouabain was prepared as a 15 mM stock in H_2O. Nimodipine and nicardipine were prepared as 10 or 100 mM stocks in ethanol. 1,3-Dipropyl-8-cyclopentylxanthine (DPCPX) was prepared as a 100 μM stock in EtOH. TPEN and (+)-5-methyl-10,11-dihydro-5*H*-dibenzo[a,d]cyclohepten-5,10-imine hydrogen maleate (MK801) stocks were in DMSO. Vehicle controls were conducted throughout for matched levels of DMSO and showed no effect on SD. All other stocks were prepared in ACSF. Most drugs were applied for 30 min before beginning challenge with ouabain, or other SD stimuli. Freshly prepared TPEN was preexposed for 10 min. High-K^+-SD was produced by delivering brief pulses from a patch electrode (3–5 MΩ) placed on the surface of the slice, ~350 μm from the recording electrode. KCl (1 M) was ejected by using a single brief pressure pulse (10 psi, 100 ms; Picrospritzer II).

Statistical analysis. Significant differences between group data were evaluated using unpaired Student's *t* tests or one-way ANOVA. Bonferroni's multiple-comparison test was used for *post hoc* analysis in which the effects of multiple drug treatments were compared against each other. Dunnett's multiple-comparison test was used for *post hoc* comparisons of multiple time points of single drug treatment, when compared with responses immediately before drug treatment. A value of $p < 0.05$ was considered significant in all cases.

Results

L-type channels can contribute to SD

A low concentration of ouabain (30 μM) reliably produced SD in acutely prepared hippocampal slices maintained at 35°C (7.9 ± 0.9 min latency; $n = 13$). Figure 1*A* shows an example of the rapid negative voltage deflection recorded with an extracellular electrode. This event is characteristic of SD and is similar to previous reports examining sustained ouabain exposures in rodent hippocampal slices (Basarsky et al., 1998; Obeidat and Andrew, 1998; Balestrino et al., 1999; Menna et al., 2000). The progression of the event was confirmed in all experiments by visualization of a spreading wave of tissue autofluorescence decrease that was coincident with the voltage deflection (Hashimoto et al., 2000;

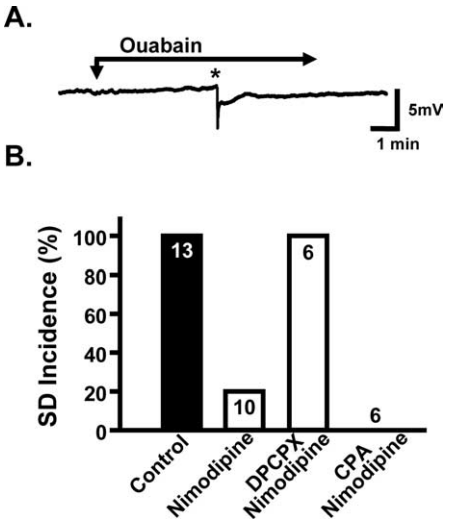

Figure 1. Nimodipine can block SD. ***A***, Example of SD triggered by ouabain (30 μM; 35°C). The sharp voltage deflection (asterisk) characteristic of SD was recorded with an extracellular electrode placed in the stratum radiatum. ***B***, Effectiveness of nimodipine depended on A_1 receptor activation. Block of A_1 receptors with DPCPX (100 nM) prevented nimodipine block of SD. Conversely, preexposure to the A_1 agonist CPA (300 nM) improved the effectiveness of nimodipine block.

Shuttleworth et al., 2003) (supplemental data, available at www.jneurosci.org as supplemental material). Figure 1*B* shows that an L-type Ca^{2+} channel blocker (nimodipine; 10 μM) prevented SD in most (80%) preparations tested.

Because both presynaptic and postsynaptic events may contribute to the onset of SD, we tested whether the level of synaptic activation in the slice might influence the effectiveness of L-type block. We used an A_1 receptor agonist [N^6-cyclopentyladenosine (CPA); 300 nM] to strongly decrease synaptic efficacy. This concentration was sufficient to abolish evoked EPSPs in CA1 stratum radiatum (data not shown), and under these conditions, nimodipine always blocked SD (six of six preparations tested) (Fig. 1*B*). Conversely, when slices were pretreated with an A_1 receptor antagonist (DPCPX; 100 nM) to increase presynaptic excitability, nimodipine never prevented ouabain-SD. A dependence of L-type sensitivity on endogenous A_1 receptor activation was also supported by experiments at a lower recording temperature (30°C), under which conditions extracellular adenosine accumulation is reported to be reduced (Masino and Dunwiddie, 1999). At 30°C, SD was little affected by nimodipine, unless the exogenous A_1 receptor agonist was coapplied. Thus, at 30°C, nimodipine alone blocked SD in only one of six preparations, but blocked SD in six of six slices when pretreated with CPA. Control experiments showed that CPA or DPCPX alone did not influence the propagation rate or time to ouabain-SD onset ($n = 6$ each).

The effects of nimodipine described above were mimicked by an alternative L-type Ca^{2+} channel blocker (nicardipine; 10 μM). In the presence of CPA at 35°C, nicardipine prevented SD in six of six slices and was without effect on ouabain-SD when A_1 receptors were blocked (DPCPX; six of six slices).

Previous work (Basarsky et al., 1999) showed that NMDA receptor activation contributes to the onset of ouabain-SD in rat hippocampal slices. Consistent with this observation, we found that the noncompetitive antagonist MK-801 (50 μM) prevented SD produced by 30 μM ouabain. Inhibition (no SD during observations >30 min) was observed at 35°C in the presence of CPA ($n = 6$) and also in the presence of DPCPX [no SD in five of six slices, and delayed SD (14.3 min) in one of six slices]. Together, these results suggest that NMDA receptors are a major contributor to the onset of ouabain-SD but that L-type channel flux also contributes to reaching SD threshold. Removing L-type flux is not sufficient to prevent SD when synaptic transmission is increased with DPCPX. However, blocking L-type flux alone appears sufficient to prevent reaching SD threshold under conditions that are relevant for ischemic brain injury, in which extracellular adenosine levels are elevated (Rudolphi et al., 1992).

The next sets of studies therefore investigated mechanisms that link L-type Ca^{2+} channel function to the initiation of ouabain-SD. Except where noted, recording conditions were chosen that emphasized a contribution of L-type channels (i.e., experiments were done at 35°C, and CPA was included to "clamp" slices at a high level of adenosine A_1 receptor activation, and thereby minimize the impact of slice–slice variation in endogenous adenosine levels).

L-type flux causes mitochondrial depolarization before SD

Changes in mitochondrial inner membrane potential ($\Delta\Psi_m$) during ouabain exposure were assessed in slices loaded with Rh123. Rh123 was used in the quenched mode, in which fluorescence increases represent $\Delta\Psi_m$ depolarization (see Materials and Methods). Figure 2 shows results from stratum pyramidale, in which a large and rapid $\Delta\Psi_m$ depolarization was observed coincident with the onset of SD, but in addition, a significant progressive depolarization was observed for ~5 min before ouabain-SD (Fig. 2*A*). Figure 2*B* shows that nimodipine prevented both phases of $\Delta\Psi_m$ changes during ouabain exposures. The slow initial $\Delta\Psi_m$ depolarization was abolished, and because SD was blocked, the large $\Delta\Psi_m$ depolarization associated with ouabain-SD was prevented.

Comparison of neuronal Ca^{2+} and Zn^{2+} dynamics

We examined whether intracellular Ca^{2+} and/or Zn^{2+} increases were likely responsible for the events described above. Although many Ca^{2+} indicators also demonstrate high-Zn^{2+} sensitivity when measured in free solution, a combination of factors appears to greatly diminish the apparent Zn^{2+} sensitivity of fura-based indicators when recordings are made in intact cells. These factors include the effects of relatively high indicator concentrations, competition with Ca^{2+} (Dineley et al., 2002), and possibly the influence of intracellular constituents (Marchi et al., 2000). Thus, intracellular Ca^{2+} and Zn^{2+} transients within neurons can be effectively distinguished by using combinations of fluorescent indicators (Devinney et al., 2005), and a similar approach was used here. Figure 3*A* shows an example of simultaneous measurements of intracellular Zn^{2+} and Ca^{2+} increases in the soma of a CA1 neuron coloaded with the high-affinity Zn^{2+} indicator FluoZin-3 and the low-affinity Ca^{2+} indicator fura-6F. Before the onset of ouabain-SD, there was no detectable increase in fura-6F ratio, and in addition there was no evidence of fluorescence increases in the individual signals after 350/380 nm excitation. In contrast, there was a significant increase in neuronal FluoZin-3 fluorescence, which was seen for ~5 min before SD propagated through the region (Fig. 3). Coincident with the onset of ouabain-SD, large increases in both fura-6F ratio and FluoZin-3 fluorescence were detected.

Because fura-6F might miss small Ca^{2+} elevations before SD, experiments were repeated in neurons loaded with only the high-affinity indicator fura-2. Figure 3*B* shows there was no detectable cytosolic Ca^{2+} elevation before ouabain-SD measured in these fura-2-loaded neurons, in contrast to mean FluoZin-3 fluores-

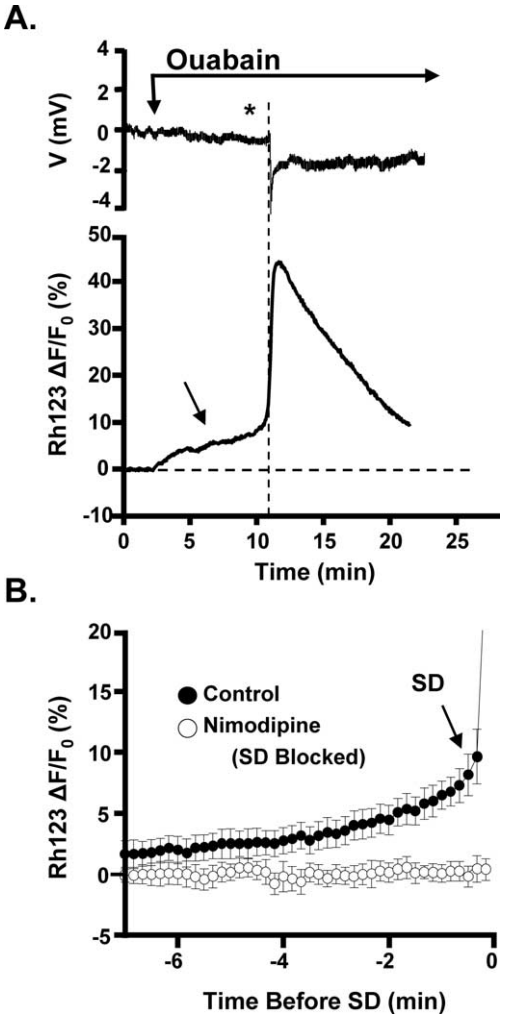

Figure 2. Mitochondrial depolarization before SD blocked by nimodipine. ***A***, Representative records showing electrically measured SD (top trace, asterisk), with Rh123 fluorescence signals monitored simultaneously from the same slice (bottom trace). Rh123 is in the quenched mode under these loading conditions, and a slow initial Rh123 fluorescence increase was observed before the sharp fluorescence increase that accompanied SD. ***B***, Mean Rh123 fluorescence increases recorded before the onset of SD. Because the time to SD onset varied between slices, measurements from seven slices have been aligned with respect to SD onset time (0 min). A slow increase in Rh123 fluorescence, interpreted as a mitochondrial depolarization, was observed before SD under control conditions (filled circles), but was not observed in slices preexposed to nimodipine (open circles; $n = 6$). Error bars indicate SEM.

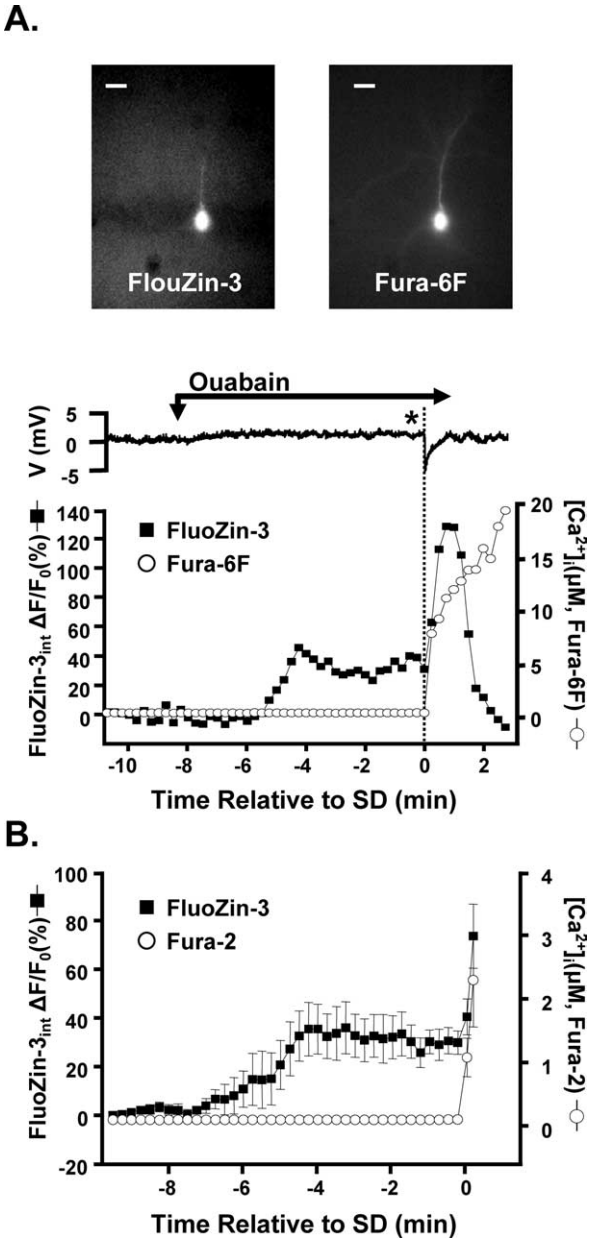

Figure 3. Neuronal Zn^{2+}, but not Ca^{2+}, increases before SD. ***A***, Fluorescence images (top) showing a representative CA1 neuron coloaded with FluoZin-3 (Ex 495 nm) and fura-6F (Ex 380 nm). The intracellular microelectrode used for loading was withdrawn before the experiment was begun. The plots are from the same preparation, and show extracellular recordings of SD (top trace, asterisk), together with FluoZin-3 (filled squares) and fura-6F (open circles) signals during ouabain exposure. Before SD, the Zn^{2+} signal increased, whereas the Ca^{2+} signal stays near basal levels. After SD, large increases in both Ca^{2+} and Zn^{2+} signals were observed. Scale bar, 10 μm. ***B***, Mean FluoZin-3 increases recorded before the onset of SD from six slices (filled squares) and mean Ca^{2+} levels measured using fura-2 from six different slices (open circles). The measurements have been aligned with respect to SD onset time (time 0) because of variance in the time to SD. Error bars indicate SEM.

cence increases, recorded from a population of different neurons. We acknowledge that the differences in apparent affinities of the indicators for Zn^{2+} and Ca^{2+} may mean that small Zn^{2+} increases may be detected by FluoZin-3 ($K_{D,Zn} \sim 15$ nM), but similar amplitude Ca^{2+} responses may still be missed in fura-2 measurements ($K_{D,Ca} \sim 225$ nM). It is also possible that somewhat larger Ca^{2+} increases may be more effectively sequestered and/or extruded by neurons (when compared with Zn^{2+}) and such differences may contribute to the differential ability to detect cytosolic Zn^{2+} versus Ca^{2+} accumulation under these conditions.

Figure 4 shows that the Zn^{2+}-selective chelator TPEN (50 μM) abolished ouabain-induced FluoZin-3 increases before SD and prevented ouabain-SD in all preparations tested under these conditions. These results suggest that (1) Zn^{2+} increases are indeed responsible for FluoZin-3 increases before SD and (2) Zn^{2+} (rather than Ca^{2+}) increases are required for SD initiation with ouabain. Consistent with these suggestions, superfusion of slices with nominally Ca^{2+}-free ACSF did not prevent ouabain-SD in six of six slices tested.

Sources of Zn^{2+} and strong correlation of early Zn^{2+} rises with subsequent SD induction

TPEN is membrane permeable and thus cannot distinguish between intracellular and extracellular sources of Zn^{2+} that might contribute to ouabain-SD. When both Ca^{2+} and Zn^{2+} were re-

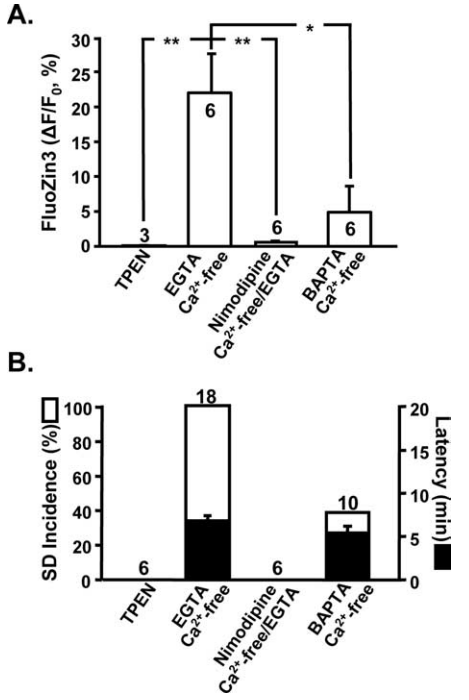

Figure 4. Sources of Zn^{2+} responsible for increases before SD, generated by ouabain. ***A***, Mean data from single neuron FluoZin-3 measurements. Slices were preexposed to TPEN (50 μM) in regular ACSF. EGTA (0.5 mM), nimodipine (10 μM), or BAPTA (1 mM) were all added in Ca^{2+}-free ACSF. TPEN and nimodipine virtually abolished pre-SD FluoZin-3 increases. EGTA did not prevent FluoZin-3 increases, but a significant decrease was observed with BAPTA. $*p < 0.05$, $**p < 0.01$, ANOVA with Bonferroni's *post hoc* tests. ***B***, Effects of the same treatments (as described for ***A***) on the incidence of SD. TPEN and nimodipine both prevented SD. EGTA did not prevent SD, whereas BAPTA reduced the susceptibility to SD to <50%. Open bars, Incidence of SD; filled bars, latency to SD. Error bars indicate SEM.

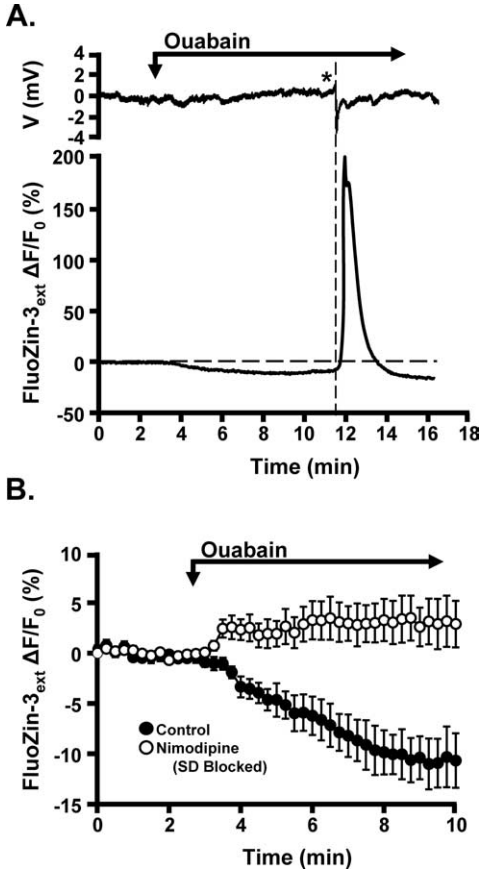

Figure 5. Extracellular Zn^{2+} decreases before SD. ***A***, Representative records showing electrically measured SD (top trace, asterisk) with plot of extracellular FluoZin-3 fluorescence (bottom trace). Before SD, the FluoZin-3 signal decreased. After SD, transient increases in the Zn^{2+} signals were observed. ***B***, Mean extracellular FluoZin-3 changes recorded before the onset of SD from five slices after ouabain (filled circles) and five slices exposed to nimodipine (10 μM) before ouabain (open circles). Nimodipine abolished the initial decrease in extracellular FlouZin-3 fluorescence and blocked SD in every case. Error bars indicate SEM.

moved from the extracellular space (superfusion with Ca^{2+}-free ACSF supplemented with 0.5 mM EGTA; $K_{D,Ca} = 10^{-8}$ M; $K_{D,Zn} = 10^{-12}$ M), there was still a significant initial FluoZin-3 increase and SD was not prevented (Fig. 4). Selective extracellular Zn^{2+} chelation with Ca^{2+}-EDTA (1 mM; $K_{D,Zn} = 10^{-16}$ M) was also ineffective at preventing either Zn^{2+} rises or SD (six of six preparations). Despite the lack of effect of these extracellular Zn^{2+} chelators, increases in FluoZin-3 fluorescence before SD were completely prevented by preexposure with nimodipine. This was demonstrated in experiments with nimodipine in Ca^{2+}-free media containing EGTA, and under these same conditions SD was always prevented (Fig. 4). Together, these results suggested that Zn^{2+} increases before ouabain-SD were mediated by L-type Ca^{2+} channels, but that the Zn^{2+} flux was not accessible to chelation by EGTA or Ca^{2+}-EDTA.

EGTA and Ca^{2+}-EDTA both have relatively slow on-rates for divalent cation binding (Smith et al., 1984; Vogt et al., 2000). We therefore tested the effects of BAPTA, which chelates both Ca^{2+} and Zn^{2+} ($K_{D,Ca} = 10^{-7}$ M; $K_{D,Zn} = 10^{-9}$ M) but with significantly faster binding kinetics (Adler et al., 1991). BAPTA blocked SD in 6 of 10 cases and significantly decreased FluoZin-3 increases before ouabain-SD (Fig. 4). These observations suggest that Zn^{2+} may accumulate outside neurons and enter through L-type channels before it can be bound by the slower extracellular chelators. One possible explanation for these observations would be a very close proximity between CA1 L-type channels and Zn^{2+} release sites.

The occurrence of transmembrane Zn^{2+} flux was further supported by measurements of extracellular FluoZin-3 fluorescence (Fig. 5). FluoZin-3 was included in ACSF, together with 1 mM Ca^{2+}-EDTA to reduce background fluorescence (Qian and Noebels, 2005) (supplemental data, available at www.jneurosci.org as supplemental material). Under these conditions, fluorescence was stable at baseline but was noted to decrease before ouabain-SD, with a time course that corresponded well with the intracellular FluoZin-3 increases signals shown above (Fig. 3). Furthermore, nimodipine preexposures that prevented SD also abolished this FluoZin-3 fluorescence decrease, consistent with the hypothesis that extracellular Zn^{2+} decreases were attributable to flux through activated L-type channels. In slices in which SD was not blocked, a large extracellular FluoZin3 increase propagated across the slice after the onset of the ouabain-SD response. Control studies showed that slice autofluorescence changes did not contaminate extracellular FluoZin-3 measurements (see supplemental data, available at www.jneurosci.org as supplemental material).

Zn^{2+} and Ca^{2+} can both contribute to the depolarization of mitochondrial inner membrane potential before SD

The findings illustrated in Figure 4 provide evidence that Zn^{2+} entry through L-type Ca^{2+} channels can play a crucial role in the induction of ouabain-SD, but do not indicate the ionic contributions to the slow $\Delta\Psi_m$ preceding SD. Indeed, as shown in Figure

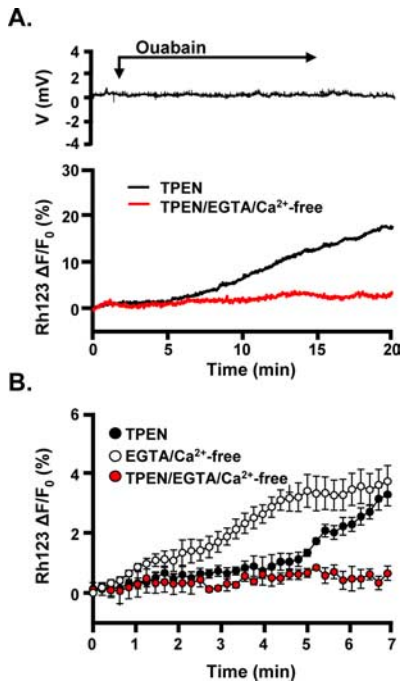

Figure 6. Zn^{2+} contributes to mitochondrial depolarization before SD. ***A***, Representative records showing the ability of TPEN (50 μM) to block SD (top trace) with corresponding preparation loaded with Rh123 (bottom trace, black line). TPEN delayed, but did not prevent slow Rh123 fluorescent increases. Combined exposure to TPEN and Ca^{2+}-free/EGTA solutions virtually abolished Rh123 increases (bottom trace, red line). ***B***, Mean Rh123 increases after that Ca^{2+}-free/EGTA solutions did not prevent an early mitochondrial depolarization before SD (black circles; $n = 6$). TPEN application delayed mitochondrial depolarization and prevented SD (red circles; $n = 6$). Chelation of both Ca^{2+} and Zn^{2+} abolished all mitochondrial depolarization (white circles; $n = 6$). Error bars indicate SEM.

6, a slow $\Delta\Psi_m$ still occurs in the presence of TPEN, which is presumably Ca^{2+} dependent, because the addition of Ca^{2+}-free/EGTA in addition to TPEN abolished the $\Delta\Psi_m$ completely. To separate Zn^{2+}- from Ca^{2+}-dependent components to the slow $\Delta\Psi_m$, we compared effects of selective Zn^{2+} removal (by TPEN) with Ca^{2+}-free/EGTA ACSF. Figure 6*B* shows that, with Ca^{2+}-free/EGTA, the slow $\Delta\Psi_m$ occurred early, whereas with selective Zn^{2+} removal it was more delayed, indicating that Zn^{2+} is the primary contributor to the earliest phase of the $\Delta\Psi_m$. Over the first 5 min after ouabain exposure, there was no significant increase in Rh123 fluorescence with TPEN, but there was a significant increase in Ca^{2+}-free/EGTA ($p < 0.01$, Dunnett's *post hoc* test). At 7 min, $\Delta\Psi_m$ significantly increased under both conditions ($p < 0.01$ for both). Indeed, suggesting that Zn^{2+} from the same extracellular source accounts for the measured Zn^{2+} rises that correlates with SD in Figure 4 and the early $\Delta\Psi_m$, both are blocked by TPEN and the fast extracellular chelator, BAPTA (data not shown for $\Delta\Psi_m$), but are not blocked by the slow extracellular chelator, EGTA.

Taking together the results from Figures 2, 3, and 6, this suggests that ouabain can lead to Ca^{2+} and Zn^{2+} influx via L-type channels and uptake by mitochondria. The high-affinity Zn^{2+} indicator FluoZin-3 appears to detect small amounts of Zn^{2+} that remain available in the cytosol, whereas cytosolic Ca^{2+} increases are not detectable. Ca^{2+}-dependent $\Delta\Psi_m$ by itself is not sufficient to cause SD. In contrast, mitochondrial uptake of Zn^{2+} is closely correlated with the onset of ouabain-SD

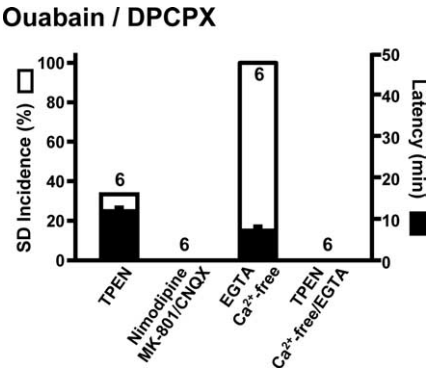

Figure 7. Effects of Zn^{2+} and Ca^{2+} removal on SD generated by ouabain. A_1 receptors were blocked with DPCPX (100 nM) in all experiments. Group data showing the incidence (open bars) and latency (filled bars) of SD. In the presence of DPCPX, TPEN blocked the occurrence of SD in four of six preparations, but Ca^{2+} removal (plus EGTA) did not block SD. In contrast, removal of both Ca^{2+} and Zn^{2+} blocked SD in six of six slices. Blocking L-type channels with nimodipine (10 μM) did not normally block SD when DPCPX was present (Fig. 1*B*), but when combined with ionotropic glutamate receptor antagonists MK-801 (50 μM) and CNQX (30 μM), SD was invariably blocked. The numbers refer to the number of slices tested under each condition. Error bars indicate SEM.

Combined effects of Zn^{2+} and Ca^{2+} when A_1 receptors were blocked

We next investigated whether Zn^{2+} was still critically required for ouabain-SD under conditions in which L-type flux was not involved. As described above (Fig. 1), nimodipine did not block SD when preparations were preexposed to DPCPX, an antagonist of A_1 receptors. This preexposure is expected to maximize presynaptic excitability and possible contributions of glutamate release to the onset of ouabain-SD. Despite the fact that L-type block was ineffective, TPEN was still quite effective in blocking SD, preventing the event in four of six preparations tested (Fig. 7). This observation suggests that, in some cases, Zn^{2+} can contribute to ouabain-SD via mechanisms other than L-type influx.

Previous studies have shown that Ca^{2+}-permeable AMPA receptors flux Zn^{2+} and can contribute to Zn^{2+}-mediated toxicity in cortical neurons (Weiss et al., 2000). We therefore tested the effects of a nonselective AMPA/KA receptor antagonist (CNQX; 30 μM) under conditions in which glutamate release should be enhanced. CNQX did not prevent ouabain-SD in DPCPX in six of six preparations (delay, 7.48 ± 0.44 min). In contrast, as noted above (see L-type channels can contribute to SD), the NMDA receptor antagonist MK801 was effective in preventing ouabain-SD in DPCPX. These results imply that Zn^{2+} influx via Ca^{2+}-permeable AMPA receptors are not responsible for Zn^{2+} increases triggering SD, and suggest that consequences of NMDA receptor activation are likely contributors for triggering ouabain-SD under these conditions. We examined Zn^{2+} increases in CA1 neurons loaded with a combination of fura-6F and FluoZin3, under conditions designed to isolate Zn^{2+} accumulation caused by non-L-type influx (DPCPX; nimodipine; Ca^{2+}-free/EGTA; 35°C). Under these conditions, a significant FluoZin-3 increase was observed in CA1 somata before SD onset (peak $\Delta F/F_0$, 16.43 ± 3.48; $p < 0.01$; $n = 5$). Consistent with the notion that these increases were attributable to NMDA receptor activation, preexposure of slices to MK801 abolished FluoZin-3 increases (mean loss of fluorescence, −8.12 ± 3.51% over the same time course; $n = 6$). The kinetics of these responses is shown in supplemental Fig. 2 (available at www.jneurosci.org as supplemental material).

Consistent with the observations above, the slow extracellular

Zn^{2+} chelator Ca^{2+}-EDTA did not block nor delay ouabain-SD during DPCPX exposure (latency, 8.45 ± 0.60 min; $n = 6$; 35°C), suggesting that the response is not attributable to contaminating Zn^{2+} in the superfusate, but rather is attributable to endogenous Zn^{2+} mobilized after NMDA receptor activation, either from intracellular sites or from extracellular sites close to influx routes.

The incomplete block of SD with TPEN (see above) also implies some involvement of Zn^{2+}-independent mechanisms, revealed by increasing presynaptic excitability with DPCPX. Under these conditions, Ca^{2+}-free/EGTA solution remained ineffective (no block or delay of SD; occurring in six of six preparations with a delay of 6.99 ± 0.93 min). However, a combination of Ca^{2+}-free/EGTA and TPEN blocked SD in six of six preparations tested. Together, these findings suggest that, although Zn^{2+}-dependent mechanisms predominate, either Zn^{2+}- or Ca^{2+}-dependent mechanisms can be sufficient to trigger SD, and a combination of these mechanisms may become more apparent when presynaptic excitability is increased.

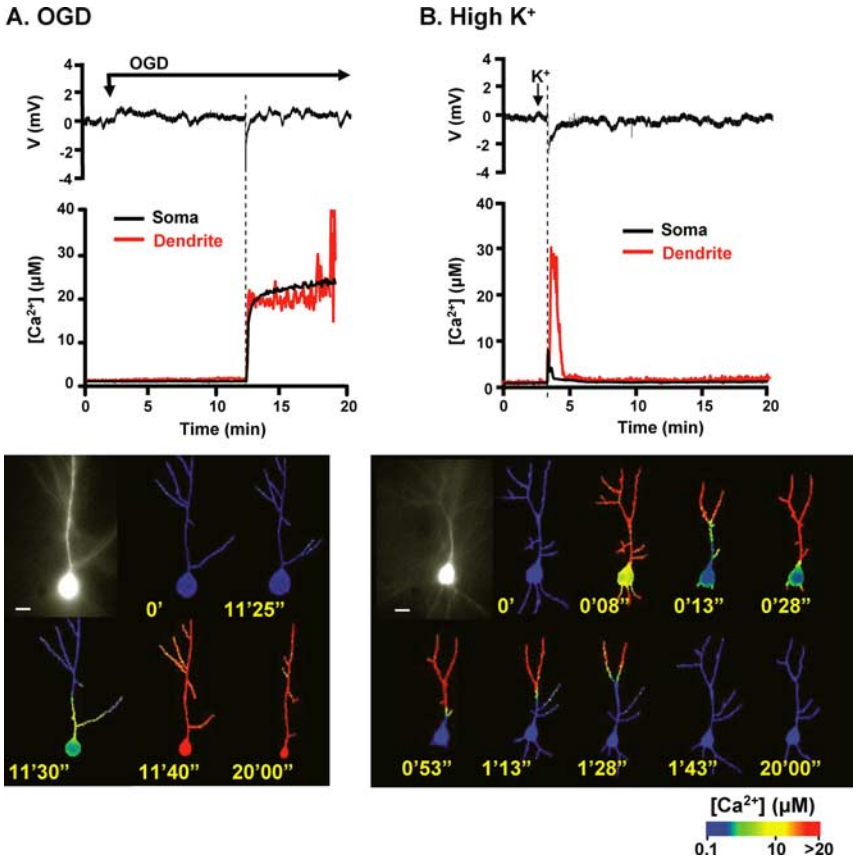

Figure 8. Ca^{2+} kinetics differ with SD stimulus. ***A***, Single CA1 neuron loaded with Ca^{2+} indicator fura-6F via sharp microelectrode exposed to OGD. The first panel shows raw 380 nm fluorescence and subsequent panels are pseudocolor images that represent intracellular [Ca^{2+}]. Intracellular Ca^{2+} levels stay near basal levels until SD hits ~11.5 min after OGD exposure. Concurrent with SD, excessive Ca^{2+} loading is evident first in the soma, and then progresses throughout dendritic processes. Simultaneous extracellular voltage recording and somatic (black) and dendritic (red) [Ca^{2+}] from the preparation are shown below. [Ca^{2+}] stays high until recording is stopped. ***B***, Ca^{2+} kinetics are very different in response to SD elicited by K^+. Approximately 8 s after K^+ application, Ca^{2+} in the entire neuron goes to low micromolar levels, but the soma quickly recovers. This is followed by high Ca^{2+} levels arising in distal dendrites that approach the soma but retreat before reaching the cell body. The Ca^{2+} within the cell returns to near-basal levels. The recordings from this cell are shown below, showing the different kinetics compared with the OGD cell in ***A*** despite the similarity in the extracellular voltage recordings. Times in the panels are relative to onset of stimulus. Scale bar, 10 μm.

SD triggered by OGD or high K^+

Having established that Zn^{2+} can contribute to SD generated by ouabain, a final series of studies examined whether Zn^{2+} was also a contributor to SD triggered by other types of stimuli. The following two test stimuli were chosen: (1) OGD and (2) localized high-K^+ applications. OGD is a model of some aspects of *in vivo* ischemic injury and produces an SD event. Previous work has shown that SD produced by either hypoxia alone (Balestrino and Somjen, 1986; Bahar et al., 2000) or OGD (Rader and Lanthorn, 1989; Tanaka et al., 1997; Obeidat and Andrew, 1998) can lead to irreversible neuronal damage, but that the propagation of these types of SD is generally not prevented by Ca^{2+} removal. In contrast, high-K^+-induced SD can generally be generated repetitively in the same preparation without obvious tissue damage (Buresová and Bures, 1969; Nedergaard and Hansen, 1988) and Ca^{2+} removal can effectively prevent the propagation of these events (Footitt and Newberry, 1998; Peters et al., 2003). We therefore tested the hypothesis that OGD-SD would be prevented by Zn^{2+} (but not Ca^{2+} removal), and the opposite would be the case for high-K^+-SD. Based on our observations with ouabain-SD, our initial studies here used concomitant A_1 receptor activation (1 μM CPA; 32°C), in an attempt to make a clear distinction between Zn^{2+}- and Ca^{2+}-dependent mechanisms.

Figure 8 shows that both OGD and localized high K^+ elicited negative shifts in extracellular potential that were similar in waveform and amplitude. Additionally, the propagation rates [as assessed by the spreading wave of tissue autofluorescence decrease described above (see L-type channels can contribute to SD)] were not significantly different between these two stimuli. Figure 8 also shows that OGD-SD Ca^{2+} signals were similar to ouabain responses. Before OGD-SD, there was no detectable increase in Ca^{2+} in six CA1 neurons, but the arrival of SD was associated with a large, irrecoverable Ca^{2+} increase that originated in somata and rapidly progressed toward apical dendrites in all neurons tested. Somatic Ca^{2+} elevations were estimated at 24.1 ± 1.1 μM ($n = 6$), and Ca^{2+} elevations throughout the neuron showed no indication of recovery after OGD-SD was generated and resulted in rapid neuronal injury. In contrast, high-K^+-SD produced a transient Ca^{2+} elevation (average increase 7.8 ± 1.9 μM in soma and 25.3 ± 2.6 μM measured in apical dendrites 40 μm from soma) that lasted <5 s. After this transient Ca^{2+} increase, an advancing front of high Ca^{2+} traveled from distal dendritic sites toward the soma. The advancing front of Ca^{2+} never fully involved the soma but instead quickly retreated out along the dendrites toward their sites of origin. Within an average of 1.7 ± 0.2 min, intracellular Ca^{2+} had recovered to >95% of resting levels. Stimulation of SD by high K^+ did not result in irreversible injury because SD could be generated repetitively by high K^+ in these preparations after 45 min recovery and a similar Ca^{2+} re-

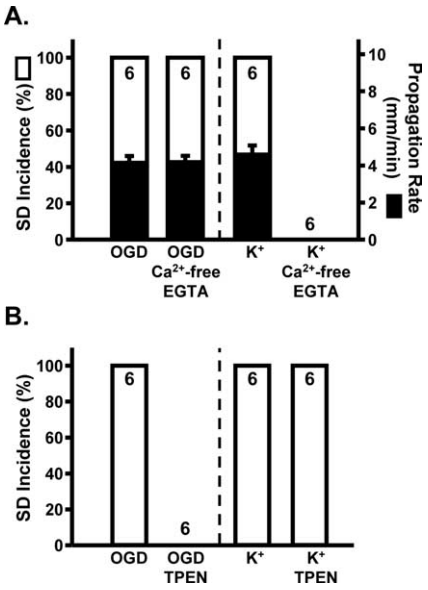

Figure 9. Effects of Ca^{2+} or Zn^{2+} removal on SD, in CPA. ***A***, Group data showing the incidence of SD evoked by either OGD (left) or K^+ (right) in Ca^{2+}-free/EGTA solution. OGD-SD showed no effect of Ca^{2+}-removal (open bars), but SD elicited by K^+ was blocked by Ca^{2+}-free media. The filled bars show that the propagation rate of the event did not change when Ca^{2+} was removed (ANOVA). ***B***, Group data showing the incidence of SD by either OGD or K^+ during Zn^{2+} chelation by TPEN. In contrast to the Ca^{2+}-free experiments in ***A***, OGD-SD was blocked by TPEN exposure, but there was no effect on the incidence of SD elicited by high K^+. CPA (300 nM) was present in all experiments, and the numbers refer to the number of slices tested under each condition. Error bars indicate SEM.

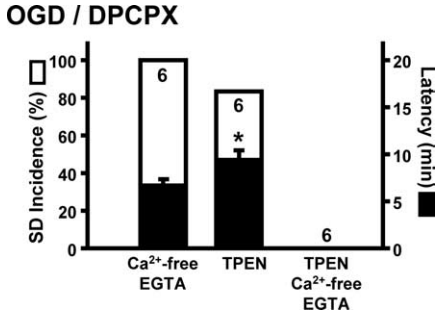

Figure 10. Effects of Zn^{2+} and Ca^{2+} removal on OGD-SD in DPCPX. Group data showing the incidence (open bars) and latency (filled bars) of SD. In the presence of DPCPX (100 nM), Ca^{2+} removal (plus EGTA) did not block OGD-SD. Similarly, the application of TPEN alone had little effect on the incidence of SD because it occurred in five of six preparations. However, the removal of both Ca^{2+} and Zn^{2+} blocked OGD-SD in six of six slices. In interleaved experiments, OGD-SD occurred in Ca^{2+}-free conditions significantly sooner than in TPEN alone ($^*p < 0.05$, unpaired *t* test). The numbers refer to the number of slices tested under each condition. Error bars indicate SEM.

sponse was produced with each SD (three of three preparations tested).

Effects of Ca^{2+} or Zn^{2+} removal on OGD-SD and high-K^+-SD

Selective removal of extracellular Ca^{2+} (plus EGTA) did not prevent the generation of OGD-SD, nor did it change the propagation rate of the spreading event when compared with responses in 2 mM Ca^{2+} in interleaved experiments (4.0 ± 0.2 vs 4.1 ± 0.4 mm/min, Ca^{2+}-free and control, respectively; $n = 6$ each; $p = 0.75$). In contrast, Ca^{2+} removal caused a profound inhibition of the propagation of SD evoked by K^+ application, in all preparations tested (Fig. 9*A*) (supplemental Fig. 3, available at www.jneurosci.org as supplemental material).

Figure 9*B* summarizes experiments showing that preexposure to the Zn^{2+} chelator TPEN (50 μM) abolished OGD-SD in all slices tested (six of six slices). In contrast, high-K^+-SD was unaffected by TPEN. High-K^+-SD occurred in all slices tested (six of six) and the time before SD onset was not changed (0.17 ± 0.04 vs 0.15 ± 0.08 min, control and TPEN, respectively; $n = 6$ each; $p = 0.75$). Thus, under these recording conditions (with A_1 receptor activation), there was a complete discrimination between Ca^{2+} and Zn^{2+} dependence of the two forms of SD; OGD-SD was entirely dependent on Zn^{2+} but unaffected by Ca^{2+} removal, whereas high-K^+-SD was entirely dependent on Ca^{2+} but unaffected by Zn^{2+} chelation.

Figure 10 shows that when A_1 receptors were blocked (DPCPX; 100 nM), Zn^{2+} remained a critical contributor to the generation of OGD-SD, but that Zn^{2+} chelation alone was no longer sufficient to prevent OGD-SD. Thus, in the presence of TPEN and DPCPX, SD was generated in five of six preparations tested. Ca^{2+} removal (plus EGTA) remained ineffective (zero of six preparations tested), but a combination of Zn^{2+} and Ca^{2+} removal blocked SD in six of six preparations tested. Together, these results suggest cooperative actions of Zn^{2+} and Ca^{2+} in triggering OGD-SD, under conditions in which synaptic activity is enhanced. An exclusive requirement for Zn^{2+}-dependent initiation can be demonstrated when presynaptic activity is reduced by either A_1 receptor activation or previous removal of extracellular Ca^{2+}.

Discussion

Zn^{2+} can contribute to SD

SD can be generated by a number of diverse stimuli and involves different mechanisms. The results here provide the first evidence that Zn^{2+} accumulation can contribute to SD initiated by the Na^+/K^+ ATPase inhibitor ouabain. Using this model, we characterized a predominant route of endogenous Zn^{2+} influx and subsequent neuronal accumulation with SD. The relevance of this finding to other types of SD was tested and showed that Zn^{2+} could be critically involved in OGD-SD, but not high-K^+-SD. The relative contributions of Zn^{2+}- and Ca^{2+}-dependent mechanisms appear to be dependent on the presynaptic excitability, because purely Zn^{2+} mechanisms are more apparent when presynaptic activity is suppressed by A_1 receptor activation, and in contrast a combination of Ca^{2+} and Zn^{2+} removal is required for abolition of SD when synaptic excitability is enhanced.

Zn^{2+}, rather than Ca^{2+} flux via L-type channels in ouabain-SD

Zn^{2+} first emerged as a candidate for SD initiation because of the mismatch between the effects of Ca^{2+} channel blockers and Ca^{2+} removal during ouabain-SD experiments (Figs. 1, 2, 4). We found conditions in which L-type channel blockers always prevented ouabain-SD, but the effects of the L-type blockers were not mimicked by removal of Ca^{2+} from the bathing medium. Likewise, mitochondrial depolarization before SD was also dependent on L-type channels, but not blocked by Ca^{2+} removal. Zn^{2+} is well established to permeate L-type channels (Weiss et al., 1993; Kerchner et al., 2000), and can contribute to mitochondrial depolarization (Sensi et al., 1999; Dineley et al., 2005), and therefore Zn^{2+} influx was considered a candidate mechanism for ouabain-SD initiation.

Neuronal Zn^{2+} increases were blocked by L-type channel blockers and were substantially attenuated by the fast extracellu-

lar Ca^{2+} and Zn^{2+} chelator, BAPTA (Adler et al., 1991), but were not affected by extracellular chelators with slow kinetics (EGTA; Ca-EDTA). Thus, these increases appear to result from Zn^{2+} accumulation in the extracellular space and rapid entry through L-type channels, before being bound by the slower chelators. Fluorescence measurements of extracellular Zn^{2+} (Fig. 5) also support extracellular sources of Zn^{2+} for the initiation of ouabain-SD, rather than liberation from intracellular binding sites. The relatively slow inactivation kinetics of L-type channels may underlie the large contribution of this particular voltage-dependent channel to Zn^{2+} influx, during prolonged depolarizations generated by ouabin exposure.

The source of the extracellular Zn^{2+} accumulation is unknown but is likely to be made up at least in part by vesicular release (Frederickson et al., 2005), for which evidence has previously been presented in the CA1 region of murine hippocampal slices (Qian and Noebels, 2005). It is also possible that other extracellular sources of Zn^{2+} contribute (Kay, 2003), but the relative contribution of different potential sources remains to be determined. Zn^{2+} accumulation was readily detected with FluoZin-3 in CA1 somata, but these experiments did not have the resolution to investigate possible increases in structures close to synaptic release sites (dendrite shafts and spines), before accumulation in somata.

Coupling Zn^{2+} flux to SD

Mitochondrial accumulation is a possible mechanism by which Zn^{2+} contributes to the induction of ouabain- or OGD-SD. Zn^{2+} uptake can induce depolarization of isolated mitochondria (Jiang et al., 2001) and mitochondria within cultured cortical neurons (Sensi et al., 2000). Notably, the studies on isolated mitochondria indicate that Zn^{2+} induces this effect with far greater potency than Ca^{2+} [10 nM for Zn^{2+} vs ~100 μM for Ca^{2+} (Jiang et al., 2001)], consistent with present indications of Zn^{2+}-dependent mitochondrial depolarization. In addition to effects on mitochondrial potential, previously described consequences of mitochondrial Zn^{2+} uptake also include reactive oxygen species production (Sensi et al., 2000), increased mitochondrial membrane permeability (Bonanni et al., 2006), and possibly compromised ATP production (Dineley et al., 2003).

NMDA receptor contributions to ouabain-SD

A prominent effect of A_1 activation is to reduce synaptic transmitter release, and the concentration of agonist (CPA) used here was sufficient to abolish evoked postsynaptic potentials. An A_1 receptor agonist was useful for characterizing the mechanisms of Zn^{2+} involvement in ouabain-SD, because it revealed a clear dependence on L-type Ca^{2+} channels and Zn^{2+} influx, without requirement for Ca^{2+}-dependent mechanisms. In contrast, when synaptic efficacy was deliberately enhanced, preventing L-type flux no longer blocked ouabain-SD, and the partial TPEN sensitivity of SD under these conditions must be explained by Zn^{2+} accumulation via other routes.

Inhibition of NMDA receptors has been reported to inhibit ouabain-SD (Basarsky et al., 1999), and we found that NMDA receptor block prevented SD triggered by 30 μM, both under conditions of increased (DPCPX) or decreased (CPA) synaptic excitability. This suggests a more dominant contribution of NMDA receptors to SD, which operates together with L-type flux. However, the relative contributions of the two pathways shifts significantly depending on the degree of synaptic excitability, such that simply removing the contribution of L-type channels is sufficient to prevent reaching SD threshold when synaptic excitability is suppressed by adenosine receptor activation. Such conditions are particularly relevant to ischemia, in which extracellular adenosine levels and A_1 activation increase significantly (Rudolphi et al., 1992).

Consistent with the hypothesis that NMDA receptor activation is primarily responsible for Zn^{2+} increases under conditions of increased excitability, MK801-sensitive FluoZin-3 increases were demonstrated in CA1 neurons, before the onset of ouabain-SD in DPCPX. These increases could involve either influx and/or liberation from intracellular Zn^{2+} buffers such as metallothionein III (Lee et al., 2003) as a consequence of NMDA receptor activation. In addition, the results suggest that additional consequences of NMDA activation (i.e., dependent on Ca^{2+} permeability) are likely to explain the triggering of SD in cases in which TPEN did not block SD, but a combination of Ca^{2+} and Zn^{2+} chelation was shown to be effective.

SD triggered by oxygen/glucose deprivation and high K^+

The relevance of Zn^{2+}-dependent mechanisms was tested using two different models, high K^+ and OGD. The SD produced by these stimuli appears very similar as it propagates across the brain slice, but the latency in onset and consequences of the SD are quite different. Similar findings have been described previously between SD evoked by hypoxia or high K^+ (Aitken et al., 1998). Figure 8 illustrates the long delay in OGD-SD and sustained Ca^{2+} overload that follows establishment of the response, in contrast to the very rapid onset of high-K^+-SD and the reversible nature of its Ca^{2+} transient. This is consistent with the irrecoverable nature of damage after persistent OGD (Rader and Lanthorn, 1989; Obeidat and Andrew, 1998; Jarvis et al., 2001) and the lack of injury after high-K^+-SD (Buresová and Bures, 1969; Nedergaard and Hansen, 1988). Previous work has established that synaptic release mechanisms are involved in recoverable forms of SD (Ayata et al., 2000; Kunkler and Kraig, 2004; van den Maagdenberg et al., 2004), and consistent with this, Ca^{2+} removal inhibited high-K^+-SD. Furthermore, Zn^{2+} chelation had no effect, implying that Zn^{2+} accumulation was not required, even when synaptic efficacy was dampened by A_1 receptor agonists.

In contrast, Zn^{2+} accumulation can be essential for OGD-SD, and this was shown when synaptic activity was suppressed by A_1 receptor activation. Under these conditions, TPEN always blocked OGD-SD, but Ca^{2+} removal was completely without effect, pointing to an essential role for Zn^{2+} under these conditions. Alternatively, when adenosine A_1 receptor activation was deliberately prevented (using DPCPX), Zn^{2+} mechanisms were no longer the only contributor required for OGD-SD, and a combination of Ca^{2+} and Zn^{2+} removal was required to prevent SD. This suggests that both Zn^{2+}-dependent and Zn^{2+}-independent mechanisms are involved and (as with ouabain) the relative contribution depends on the degree of synaptic activation.

Together, it is likely that progressive accumulation of Zn^{2+} in neurons could be an important contributor to SD in which initial membrane depolarizations are slow and progressive (OGD; ouabain), but not necessarily in other SD models in which the time course of initial depolarization is very rapid (high K^+). Previous studies have provided strong evidence that intracellular Zn^{2+} accumulation contributes substantially to injury after *in vivo* ischemia (Koh et al., 1996; Calderone et al., 2004). It is tempting to consider the possibility that one of the ways that Zn^{2+} contributes to postischemic injury is by facilitating the induction of SD-like events *in vivo*. Periinfarct depolarizations have been described after *in vivo* ischemia and propagate from the edges of infarcted regions to contribute to the spread of ischemic

injury in the hours or days after an insult (Nedergaard and Astrup, 1986; Hossmann, 1996; Hartings et al., 2003). It will be of interest to determine whether Zn^{2+} accumulation is critical for the generation of periinfarct depolarizations after ischemia *in vivo*, and whether prevention of these events could contribute to the effectiveness of delayed Zn^{2+} chelation, provided many hours after the initial insult (Calderone et al., 2004).

Conclusion

The present work provides the first evidence that endogenous Zn^{2+} can contribute to SD, and could provide a key to distinguishing between different types of SD, in different pathophysiological settings. Additional understanding of mechanisms involved in the induction of SD by Zn^{2+} and its role in propagation of injury in conditions including ischemia and trauma could help in the development of new neuroprotective strategies.

References

Adler EM, Augustine GJ, Duffy SN, Charlton MP (1991) Alien intracellular calcium chelators attenuate neurotransmitter release at the squid giant synapse. J Neurosci 11:1496–1507.

Aitken PG, Tombaugh GC, Turner DA, Somjen GG (1998) Similar propagation of SD and hypoxic SD-like depolarization in rat hippocampus recorded optically and electrically. J Neurophysiol 80:1514–1521.

Ayata C, Shimizu-Sasamata M, Lo EH, Noebels JL, Moskowitz MA (2000) Impaired neurotransmitter release and elevated threshold for cortical spreading depression in mice with mutations in the alpha1A subunit of P/Q type calcium channels. Neuroscience 95:639–645.

Bahar S, Fayuk D, Somjen GG, Aitken PG, Turner DA (2000) Mitochondrial and intrinsic optical signals imaged during hypoxia and spreading depression in rat hippocampal slices. J Neurophysiol 84:311–324.

Balestrino M, Somjen GG (1986) Chlorpromazine protects brain tissue in hypoxia by delaying spreading depression-mediated calcium influx. Brain Res 385:219–226.

Balestrino M, Young J, Aitken P (1999) Block of (Na^+,K^+)ATPase with ouabain induces spreading depression-like depolarization in hippocampal slices. Brain Res 838:37–44.

Basarsky TA, Duffy SN, Andrew RD, MacVicar BA (1998) Imaging spreading depression and associated intracellular calcium waves in brain slices. J Neurosci 18:7189–7199.

Basarsky TA, Feighan D, MacVicar BA (1999) Glutamate release through volume-activated channels during spreading depression. J Neurosci 19:6439–6445.

Bonanni L, Chachar M, Jover-Mengual T, Li H, Jones A, Yokota H, Ofengeim D, Flannery RJ, Miyawaki T, Cho CH, Polster BM, Pypaert M, Hardwick JM, Sensi SL, Zukin RS, Jonas EA (2006) Zinc-dependent multiconductance channel activity in mitochondria isolated from ischemic brain. J Neurosci 26:6851–6862.

Buresová O, Bures J (1969) The effect of prolonged cortical spreading depression on learning and memory in rats. J Neurobiol 1:135–146.

Calderone A, Jover T, Mashiko T, Noh KM, Tanaka H, Bennett MV, Zukin RS (2004) Late calcium EDTA rescues hippocampal CA1 neurons from global ischemia-induced death. J Neurosci 24:9903–9913.

Choi DW, Koh JY (1998) Zinc and brain injury. Annu Rev Neurosci 21:347–375.

Church AJ, Andrew RD (2005) Spreading depression expands traumatic injury in neocortical brain slices. J Neurotrauma 22:277–290.

Devinney MJ 2nd, Reynolds IJ, Dineley KE (2005) Simultaneous detection of intracellular free calcium and zinc using fura-2FF and FluoZin-3. Cell Calcium 37:225–232.

Dietz RM, Weiss JH, Shuttleworth CW (2007a) Intracellular Zn^{2+} increases can contribute to spreading depression in hippocampal slices. Soc Neurosci Abstr 33:55.4.

Dietz RM, Kiedrowski L, Shuttleworth CW (2007b) Contribution of Na^+/Ca^{2+} exchange to excessive Ca^{2+} loading in dendrites and somata of CA1 neurons in acute slice. Hippocampus 17:1049–1059.

Dineley KE, Malaiyandi LM, Reynolds IJ (2002) A reevaluation of neuronal zinc measurements: artifacts associated with high intracellular dye concentration. Mol Pharmacol 62:618–627.

Dineley KE, Votyakova TV, Reynolds IJ (2003) Zinc inhibition of cellular energy production: implications for mitochondria and neurodegeneration. J Neurochem 85:563–570.

Dineley KE, Richards LL, Votyakova TV, Reynolds IJ (2005) Zinc causes loss of membrane potential and elevates reactive oxygen species in rat brain mitochondria. Mitochondrion 5:55–65.

Duchen MR, Surin A, Jacobson J (2003) Imaging mitochondrial function in intact cells. Methods Enzymol 361:353–389.

Footitt DR, Newberry NR (1998) Cortical spreading depression induces an LTP-like effect in rat neocortex in vitro. Brain Res 781:339–342.

Frederickson CJ, Koh JY, Bush AI (2005) The neurobiology of zinc in health and disease. Nat Rev Neurosci 6:449–462.

Gerich FJ, Hepp S, Probst I, Müller M (2006) Mitochondrial inhibition prior to oxygen-withdrawal facilitates the occurrence of hypoxia-induced spreading depression in rat hippocampal slices. J Neurophysiol 96:492–504.

Hadjikhani N, Sanchez Del Rio M, Wu O, Schwartz D, Bakker D, Fischl B, Kwong KK, Cutrer FM, Rosen BR, Tootell RB, Sorensen AG, Moskowitz MA (2001) Mechanisms of migraine aura revealed by functional MRI in human visual cortex. Proc Natl Acad Sci U S A 98:4687–4692.

Hartings JA, Rolli ML, Lu XC, Tortella FC (2003) Delayed secondary phase of peri-infarct depolarizations after focal cerebral ischemia: relation to infarct growth and neuroprotection. J Neurosci 23:11602–11610.

Hashimoto M, Takeda Y, Sato T, Kawahara H, Nagano O, Hirakawa M (2000) Dynamic changes of NADH fluorescence images and NADH content during spreading depression in the cerebral cortex of gerbils. Brain Res 872:294–300.

Hossmann KA (1996) Periinfarct depolarizations. Cerebrovasc Brain Metab Rev 8:195–208.

Jarvis CR, Anderson TR, Andrew RD (2001) Anoxic depolarization mediates acute damage independent of glutamate in neocortical brain slices. Cereb Cortex 11:249–259.

Jiang D, Sullivan PG, Sensi SL, Steward O, Weiss JH (2001) Zn^{2+} induces permeability transition pore opening and release of pro-apoptotic peptides from neuronal mitochondria. J Biol Chem 276:47524–47529.

Kay AR (2003) Evidence for chelatable zinc in the extracellular space of the hippocampus, but little evidence for synaptic release of Zn. J Neurosci 23:6847–6855.

Kerchner GA, Canzoniero LM, Yu SP, Ling C, Choi DW (2000) Zn^{2+} current is mediated by voltage-gated Ca^{2+} channels and enhanced by extracellular acidity in mouse cortical neurones. J Physiol 528:39–52.

Koh JY, Suh SW, Gwag BJ, He YY, Hsu CY, Choi DW (1996) The role of zinc in selective neuronal death after transient global cerebral ischemia. Science 272:1013–1016.

Kunkler PE, Kraig RP (2004) P/Q Ca^{2+} channel blockade stops spreading depression and related pyramidal neuronal Ca^{2+} rise in hippocampal organ culture. Hippocampus 14:356–367.

Lee JY, Kim JH, Palmiter RD, Koh JY (2003) Zinc released from metallothionein-iii may contribute to hippocampal CA1 and thalamic neuronal death following acute brain injury. Exp Neurol 184:337–347.

Malaiyandi LM, Vergun O, Dineley KE, Reynolds IJ (2005) Direct visualization of mitochondrial zinc accumulation reveals uniporter-dependent and -independent transport mechanisms. J Neurochem 93:1242–1250.

Marchi B, Burlando B, Panfoli I, Viarengo A (2000) Interference of heavy metal cations with fluorescent Ca^{2+} probes does not affect Ca^{2+} measurements in living cells. Cell Calcium 28:225–231.

Masino SA, Dunwiddie TV (1999) Temperature-dependent modulation of excitatory transmission in hippocampal slices is mediated by extracellular adenosine. J Neurosci 19:1932–1939.

Menna G, Tong CK, Chesler M (2000) Extracellular pH changes and accompanying cation shifts during ouabain-induced spreading depression. J Neurophysiol 83:1338–1345.

Nedergaard M, Astrup J (1986) Infarct rim: effect of hyperglycemia on direct current potential and [^{14}C]2-deoxyglucose phosphorylation. J Cereb Blood Flow Metab 6:607–615.

Nedergaard M, Hansen AJ (1988) Spreading depression is not associated with neuronal injury in the normal brain. Brain Res 449:395–398.

Obeidat AS, Andrew RD (1998) Spreading depression determines acute cellular damage in the hippocampal slice during oxygen/glucose deprivation. Eur J Neurosci 10:3451–3461.

Peters O, Schipke CG, Hashimoto Y, Kettenmann H (2003) Different mechanisms promote astrocyte Ca^{2+} waves and spreading depression in the mouse neocortex. J Neurosci 23:9888–9896.

Qian J, Noebels JL (2005) Visualization of transmitter release with zinc fluorescence detection at the mouse hippocampal mossy fibre synapse. J Physiol 566:747–758.

Rader RK, Lanthorn TH (1989) Experimental ischemia induces a persistent depolarization blocked by decreased calcium and NMDA antagonists. Neurosci Lett 99:125–130.

Ramos JG (1975) Ionic movements in the isolated chicken retina during spreading depression. Acta Physiol Lat Am 25:112–119.

Rudolphi KA, Schubert P, Parkinson FE, Fredholm BB (1992) Neuroprotective role of adenosine in cerebral ischaemia. Trends Pharmacol Sci 13:439–445.

Sensi SL, Yin HZ, Carriedo SG, Rao SS, Weiss JH (1999) Preferential Zn^{2+} influx through Ca^{2+}-permeable AMPA/kainate channels triggers prolonged mitochondrial superoxide production. Proc Natl Acad Sci U S A 96:2414–2419.

Sensi SL, Yin HZ, Weiss JH (2000) AMPA/kainate receptor-triggered Zn^{2+} entry into cortical neurons induces mitochondrial Zn^{2+} uptake and persistent mitochondrial dysfunction. Eur J Neurosci 12:3813–3818.

Shuttleworth CW, Connor JA (2001) Strain-dependent differences in calcium signaling predict excitotoxicity in murine hippocampal neurons. J Neurosci 21:4225–4236.

Shuttleworth CW, Brennan AM, Connor JA (2003) NAD(P)H fluorescence imaging of postsynaptic neuronal activation in murine hippocampal slices. J Neurosci 23:3196–3208.

Smith PD, Liesegang GW, Berger RL, Czerlinski G, Podolsky RJ (1984) A stopped-flow investigation of calcium ion binding by ethylene glycol bis(beta-aminoethyl ether)-*N*,*N*′-tetraacetic acid. Anal Biochem 143:188–195.

Somjen GG (2001) Mechanisms of spreading depression and hypoxic spreading depression-like depolarization. Physiol Rev 81:1065–1096.

Tanaka E, Yamamoto S, Kudo Y, Mihara S, Higashi H (1997) Mechanisms underlying the rapid depolarization produced by deprivation of oxygen and glucose in rat hippocampal CA1 neurons in vitro. J Neurophysiol 78:891–902.

Umegaki M, Sanada Y, Waerzeggers Y, Rosner G, Yoshimine T, Heiss WD, Graf R (2005) Peri-infarct depolarizations reveal penumbra-like conditions in striatum. J Neurosci 25:1387–1394.

van den Maagdenberg AM, Pietrobon D, Pizzorusso T, Kaja S, Broos LA, Cesetti T, van de Ven RC, Tottene A, van der Kaa J, Plomp JJ, Frants RR, Ferrari MD (2004) A Cacna1a knockin migraine mouse model with increased susceptibility to cortical spreading depression. Neuron 41:701–710.

Vogt K, Mellor J, Tong G, Nicoll R (2000) The actions of synaptically released zinc at hippocampal mossy fiber synapses. Neuron 26:187–196.

Weiss JH, Hartley DM, Koh JY, Choi DW (1993) AMPA receptor activation potentiates zinc neurotoxicity. Neuron 10:43–49.

Weiss JH, Sensi SL, Koh JY (2000) Zn^{2+}: a novel ionic mediator of neural injury in brain disease. Trends Pharmacol Sci 21:395–401.

Young JN, Somjen GG (1992) Suppression of presynaptic calcium currents by hypoxia in hippocampal tissue slices. Brain Res 573:70–76.